

Infrared Hall conductivity in optimally doped $\text{Bi}_2\text{Sr}_2\text{CaCu}_2\text{O}_{8+\delta}$: Drude behavior examined by experiment and fluctuation-exchange-model calculations

D. C. Schmadel,^{1,*} G. S. Jenkins,^{1,*} J. J. Tu,^{2,3} G. D. Gu,³ Hiroshi Kontani,⁴ and H. D. Drew^{1,5}

¹*Department of Physics, University of Maryland, College Park, Maryland 20742, USA*

²*Department of Physics, City University of New York, New York, New York 11973, USA*

³*Department of Physics, Brookhaven National Laboratory, Upton, New York 11973, USA*

⁴*Department of Physics, Nagoya University, Furo-cho, Nagoya 464-8602, Japan*

⁵*Center of Superconductivity Research, University of Maryland, College Park, Maryland 20742, USA*

(Received 6 December 2006; published 16 April 2007)

The temperature dependence of the Hall conductivity is reported at mid- and far-IR frequencies for cleaved single crystals. A nearly simple Drude behavior is observed with a scattering rate that is linear in temperature and nearly frequency independent. The Hall data are in good agreement with calculations based on the fluctuation-exchange interaction when current vertex corrections are included. The σ_{xy} quasiparticle spectral weight is suppressed to 0.09 times the band value, compared with 0.33 times the band value for σ_{xx} .

DOI: [10.1103/PhysRevB.75.140506](https://doi.org/10.1103/PhysRevB.75.140506)

PACS number(s): 74.72.Hs, 71.18.+y, 74.20.Mn, 74.25.Nf

While significant progress has been made toward an understanding of the cuprate superconductors due in large part to important new experimental data from angle-resolved photoemission spectroscopy (ARPES), neutron scattering, and IR measurements, a clear microscopic theory remains elusive. Indeed, a theory of the superconductivity and transport properties of these strongly correlated materials continues as a central problem in modern condensed matter physics. The correlations with magnetic fluctuations have been elucidated by neutron scattering,¹ and the nature and occurrence of quasiparticles near the Fermi surface and in different phases have been mapped by ARPES.² Evidence is accumulating that the underdoped cuprates, particularly electron-doped materials, support spin density waves which partially gap the Fermi surface.^{3,4} The optimally doped cuprates, however, are found to have a large nearly circular Fermi surface with quasiparticles that are well defined in the (π, π) direction and somewhat less well defined in the $(\pi, 0)$ direction. The linear temperature-dependent resistivity is found to correspond to the linearly temperature-dependent quasiparticle imaginary self-energy. At optimal doping the cuprates do not exhibit significant evidence for the pseudogap observed in underdoped materials.⁵ Nevertheless, anomalous transport properties of the nearly optimally doped cuprates are universally observed. One such anomaly is the temperature dependence of the Hall coefficient which has frequently been cited as evidence of the non-Fermi-liquid character of the cuprates.

One important approach to understanding the magnetotransport anomalies as well as other transport anomalies of the cuprates is to include vertex corrections in the conductivity within Fermi liquid theory. Kontani and Yamada⁶ have examined this approach using the spin fluctuation exchange interaction between carriers and include current vertex corrections in the conductivity. They find that the current vertex corrections enter into σ_{xy} more significantly than in σ_{xx} and that this theory is capable of explaining the anomalous dc magnetotransport of the optimally doped cuprates in terms of the temperature dependence of the spin-fluctuation-induced interaction. More recently, Kontani⁷ has examined the IR

frequency dependence of magnetotransport with further success, which further highlights the possibility that strong correlations may enter the diagonal and off-diagonal conductivities differently. This insight suggests that σ_{xy} may be a more useful quantity to study than the Hall angle $\theta_H = \sigma_{xy} / \sigma_{xx}$. In this work we examine the temperature dependence of σ_{xy} in optimally doped $\text{Bi}_2\text{Sr}_2\text{CaCu}_2\text{O}_{8+\delta}$ [BSCCO(2212)] which does not have conduction by chains that complicated the interpretation of the IR Hall data for $\text{YBa}_2\text{Cu}_3\text{O}_7$ of earlier work.⁸ We find that, for frequencies around 10 meV and 100 meV, σ_{xy} is consistent with a nearly simple Drude form in contrast to both σ_{xx} and θ_H . The parameters of the Drude form are evaluated and compared with other transport properties, with theoretical calculations based on Kontani⁷ and with the σ_{xy} sum rule.

The experimental system of the current work measures the very small complex Faraday angle imparted to CO_2 laser radiation traveling perpendicular to and transmitted by the sample, which is immersed in a magnetic field also perpendicular to its surface. The system is the same as that used by in the earlier YBCO study⁸ with the addition of an in-line calibration system and a continuous stress-free temperature scan provision.⁹ The sample of the current work was cleaved, or rather peeled, from a bulk single crystal of $\text{Bi}_2\text{Sr}_2\text{CaCu}_2\text{O}_{8+\delta}$ grown by the traveling floating zone method.¹⁰ The resulting 100-nm-thick film was placed in thermal contact with a supporting wedged BaF_2 substrate. Measurement of the ac magnetic susceptance of this mounted, peeled segment revealed a T_c of 92 K with a width of less than 1 K. This measurement was performed after all of the Hall measurements had been completed, thus establishing the integrity of the sample and recommending the Hall data as representative of optimally doped BSCCO. The far-infrared measurements were performed on a similarly peeled sample of BSCCO mounted onto a quartz substrate. The measurement apparatus used a molecular vapor laser as the source and a detection system similar to that of Grayson *et al.*¹¹ Infrared conductivity data,¹² from measurements performed on bulk crystals from the same batch, supplied the real and imaginary parts of of the longitudinal conductivity

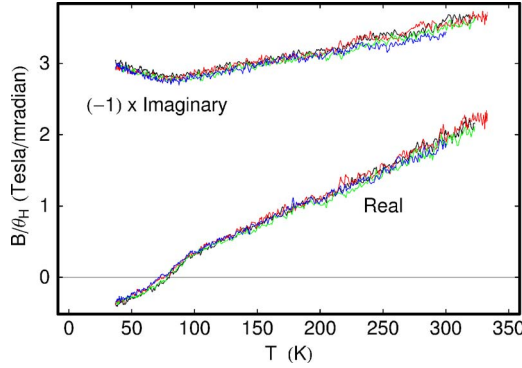


FIG. 1. (Color online) The real and imaginary parts of the inverse Hall angle θ_H^{-1} for 2212 BSCCO versus temperature measured at 950 cm^{-1} and normalized to 1 T from four pairs of temperature scans.

σ_{xx} required to obtain the Hall angle and the transverse conductivity σ_{xy} from the measured Faraday angle.⁹ Figure 1 shows the results for the midinfrared from four pairs of temperature scans.

We may analyze the results using the extended Drude model

$$\sigma_{xx} = \frac{S_{xx}}{\gamma_{xx} - i\omega[1 + \lambda(T, \omega)]} = \frac{S_{xx}^*}{\gamma_{xx}^* - i\omega}, \quad (1)$$

$$\sigma_{xy} = \frac{S_{xy}}{\{\gamma_{xy} - i\omega[1 + \lambda(T, \omega)]\}^2} = \frac{S_{xy}^*}{(\gamma_{xy}^* - i\omega)^2}, \quad (2)$$

where S_{xx} and S_{xy} are the longitudinal and transverse spectral weights¹³ defined here as

$$S_{xx} = \int_0^{\Omega_c} \frac{2}{\pi} \text{Re } \sigma_{xx} d\omega, \quad (3)$$

$$S_{xy} = \int_0^{\Omega_c} \frac{2}{\pi} \omega \text{Im } \sigma_{xy} d\omega, \quad (4)$$

where Ω_c as a cutoff frequency high enough that the imaginary part of the quasiparticle self-energy is saturated but still below the Mott-Hubbard gap. The measured quantities in the IR Hall experiment at fixed frequency actually relate to $S_{xy}^* = [\omega / \text{Im}(\sigma_{xy}^{-1/2})]^2 = S_{xy}(1 + \lambda_{xy})^{-2}$ and $\gamma_{xy}^* = \gamma_{xy} / (1 + \lambda_{xy})$. This form recognizes the fact that the longitudinal and transverse scattering rates γ_{xx}^* and γ_{xy}^* may be different. In fact, attempts to analyze the data under the assumption that they are identical leads to nonphysical results. Consider that with $\gamma_{xy}^* = \gamma_{xx}^* = \gamma^*$, then from $\theta_H = \sigma_{xy} / \sigma_{xx}$

$$\theta_H^{-1} = \frac{\gamma^*}{\omega_H^*} - \frac{\omega}{\omega_H^*}, \quad (5)$$

where $\omega_H^* = S_{xy}^* / S_{xx}^*$. From Fig. 1 we see that Eq. (5) implies a normal-state scattering rate with a negative projection below 50 K and a Hall mass of $2.9m_e$, which, though similar in magnitude to the ARPES-measured mass, increases with temperature. Such unconventional results challenge this simple analysis and suggest that the effective longitudinal

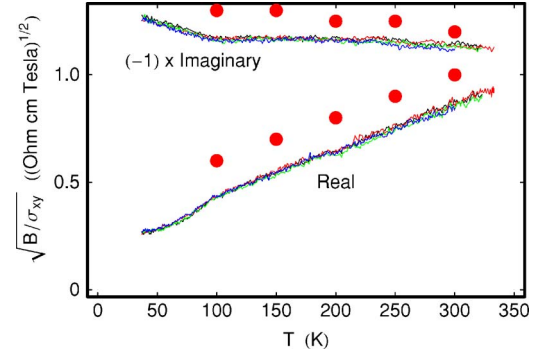


FIG. 2. (Color online) $\sigma_{xy}^{-1/2}$ for 2212 BSCCO at 300 K versus temperature measured at 950 cm^{-1} and normalized to 1 T. The solid dots are the calculated results of the FLEX+CVC (Ref. 14) approximation.

and transverse scattering rates are different. Therefore in this paper we examine the transverse conductivity σ_{xy} independently.

Figure 2 displays the data in terms of σ_{xy} . The renormalized transverse scattering rate from Eq. (2) is simply

$$\gamma_{xy}^* = -\omega \frac{\text{Re}(\sigma_{xy}^{-1/2})}{\text{Im}(\sigma_{xy}^{-1/2})}. \quad (6)$$

This alternative analysis of the data results in a transverse scattering rate γ_{xy}^* which is everywhere positive, increases linearly with temperature and has a zero temperature projection of 200 cm^{-1} . This analysis also results in a transverse spectral weight which increases slightly with temperature. Remarkably, this observed temperature behavior of the transverse conductivity is well captured by the calculated results of the fluctuation exchange approximation with current vertex corrections (FLEX+CVC)¹⁴ for $\text{La}_{2-x}\text{Sr}_x\text{CuO}_4$ at 10% doping shown as solid circles in Fig. 2. Similar results are obtained for $\text{YBa}_2\text{Cu}_3\text{O}_x$ calculations. In the relaxation time approximation, where the CVC is dropped, $\text{Re}(\sigma_{xy}^{-1/2}) \propto \gamma(\omega)$ and is approximately temperature independent for $\hbar\omega \gg k_B T$. According to the calculations, the approximate linear temperature behavior of $\text{Re}(\sigma_{xy}^{-1/2})$ is caused by the CVC due to spin fluctuations, which are strongly temperature dependent. The existence of the CVC is a consequence of conservation laws, which intimately govern the transport phenomena. Consequently, neglecting the CVC frequently leads to nonphysical predictions. In these calculated results the vertex corrections enter into σ_{xx} quite differently from σ_{xy} . Although the CVC is less effective as the doping increases, a similar numerical result is obtained even at 15% doping if we use a larger value of the Coulomb interaction U , which is the single adjustable parameter of the theory.

Additionally, the FLEX+CVC approximation captures the frequency behavior of the transverse conductivity as well. To examine this frequency dependence we introduce the data shown in Fig. 3 for optimally doped BSCCO at 84 cm^{-1} . Measurements were also performed at 24 and 42 cm^{-1} and proved to be consistent with those shown. These far-infrared data, multiplied by σ_{xx} to produce σ_{xy} ,

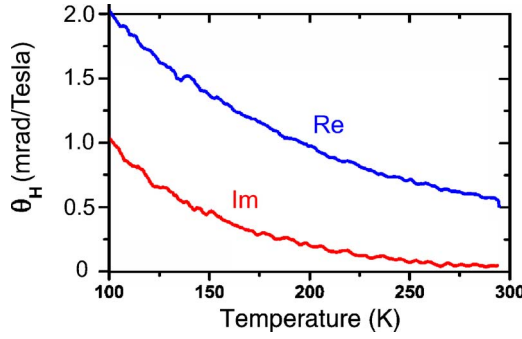


FIG. 3. (Color online) θ_H for optimally doped 2212 BSCCO versus temperature measured at 84 cm^{-1} averaged from five thermal scans and normalized to 1 T.

appear in Fig. 4 along with the midinfrared data and two frequency points from the FLEX+CVC calculations.

Since $\text{Im}(\sigma_{xy}^{-1/2})/\omega$ is found to be nearly independent of temperature and frequency over the measured infrared range, it is interesting to consider the observed values in more general terms. The extended Drude model in Eq. (2) relates $\text{Im}(\sigma_{xy}^{-1/2})$ to the Drude spectral weight. Generally, for strongly interacting systems near a Mott transition, one expects $\lambda_{xy} \rightarrow 0$ and γ_{xy} to saturate at frequencies $\omega_s < \Omega_c$ as the measurement frequency exceeds the saturation frequency (typically $\sim 400 \text{ meV}$ for cuprates) while still remaining below the Mott-Hubbard gap. This is the observed behavior of $\sigma_{xx}(\omega)$ in the optimally hole doped cuprates.¹⁵

Assuming the same interaction energy scale for the transverse conductivity, the data allow us to characterize the Drude peak in σ_{xy} , which is at a frequency $\omega \approx \gamma_{xy}^*$. We can compare S_{xy}^* and γ_{xy}^* at far-IR and mid-IR frequencies obtained from Eq. (2). The results are shown in Table I, which summarizes experimental results in terms of the scattering rates and spectral weights along with the longitudinal scattering rates from σ_{xx}^* . In the table, $\gamma_{xy}^*(84)$ is comparable to $\gamma_{xx}^*(84)$; however, $\gamma_{xy}^*(950)$ is much less than $\gamma_{xx}^*(950)$, corresponding to a weaker frequency-dependent scattering. Therefore, we expect $\lambda_{xy} < \lambda_{xx}$, and since $\lambda_{xx} < 1$ at 950 cm^{-1} , we expect $\lambda_{xy} \ll 1$. This suggests that $S_{xy}^* = S_{xy}(1 + \lambda_{xy})^{-2} \approx S_{xy}$ so that S_{xy}^* in the mid-IR frequencies

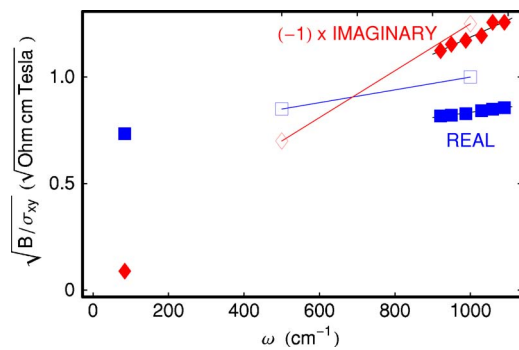


FIG. 4. (Color online) $\sigma_{xy}^{-1/2}$ for 2212 BSCCO at 300 K and normalized to 1 T. The data are shown as solid squares (real) and solid diamonds (imaginary), and the FLEX+CVC calculations are represented by open squares (real) and open diamonds (imaginary).

TABLE I. (Color online) Renormalized scattering rates in cm^{-1} for the longitudinal and transverse conductivity and the spectral weights in seconds^{-3} per tesla at far-IR (84 cm^{-1}) and mid-IR (950 cm^{-1}) frequencies at different temperatures.

T (K)	$\gamma_{xx}^*(84)^a$	$\gamma_{xx}^*(950)^a$	$\gamma_{xy}^*(84)$	$\gamma_{xy}^*(950)$	$S_{xy}^*(84)$	$S_{xy}^*(950)$
100	130	660	150	350	2.0×10^{40}	2.1×10^{40}
200	400	920	400	530	2.4×10^{40}	2.1×10^{40}
300	600	1070	690	720	2.8×10^{40}	2.3×10^{40}

^aReference 16.

should give a good approximate measure of the Drude contribution to the σ_{xy} sum rule. Further support for this is obtained by comparing S_{xy}^* in the mid- and far-IR frequencies from the table. It is seen that they are in good agreement, again consistent with a very weak frequency dependence of the optical self-energy $\Sigma_{xy}(\omega) = \omega\lambda_{xy} + i\gamma_{xy}$ and $\lambda_{xy} \ll 1$. In fact these results indicate that σ_{xy} has very nearly a simple Drude form in optimally doped BSCCO.

Since this analysis of the far-IR and mid-IR data appears to provide a measure of the partial sum S_{xy} , it is interesting to compare the value to the band value which can be calculated from the general relation¹³

$$S_{xy}^{\text{band}} = e^3 B \sum_k \det(m_k^{-1}) n_k, \quad (7)$$

where

$$m_k^{-1} = \frac{\partial^2 E(k)}{\hbar^2 \partial k \partial k} \quad (8)$$

is the inverse mass tensor and n_k is the Fermi function. To calculate S_{xy}^{band} we use the tight-binding fit to the cuprate band structure:³

$$E(k_x, k_y) = -2t_1[\cos(k_x) + \cos(k_y)] + 4t_2 \cos(k_x)\cos(k_y) - 2t_3[\cos(2k_x) + \cos(2k_y)], \quad (9)$$

where $t_1 = 0.38 \text{ eV}$, $t_2 = 0.32t_1$, and $t_3 = 0.5t_2$. At optimal doping, the electron density n is 0.84 and $S_{xy}^{\text{band}} = 3.73 \times 10^{41} \text{ Hz}^3/\text{T}$ and so $S_{xy}^*/S_{xy}^{\text{band}} = 0.09$. It is interesting to compare this observed reduction from S_{xy}^{band} with the behavior of $S_{xx} = \omega_p^2/4\pi$, where ω_p is the bare plasma frequency. Using the band model we find $S_{xx}^{\text{band}} = \frac{e^2}{2} \sum_k \text{tr}(m_k^{-1}) n_k = 3.50 \times 10^{30} \text{ Hz}$.² From the literature^{12,16} $\omega_p = 16 \text{ 200 cm}^{-1}$ so that $S_{xx}^*/S_{xx}^{\text{band}} = 0.33$. This compares with similar estimations for single layer $\text{Pr}_{2-x}\text{Ce}_x\text{CuO}_4$ and $\text{L}_{2-x}\text{Sr}_x\text{CO}_4$.³ Therefore we see that S_{xy}^* is more significantly suppressed than S_{xx}^* . Indeed, $S_{xy}^*/S_{xy}^{\text{band}} \approx (S_{xx}^*/S_{xx}^{\text{band}})^2$. If interpreted as an effective mass, then $S_{xy}/S_{xx} = \omega_H$ and $m_H/m_0 = 6.7$. The reduction in S_{xx} is associated with the Coulomb correlations due to the proximity to the Mott transition as has been discussed recently.³ There are no theoretical results for S_{xy} . However, whether the reduction is to be thought of as a mass effect or a charge effect in Fermi liquid theory, a larger reduction of S_{xy} may be expected as $S_{xx} \sim e^2/m$ and $S_{xy} \sim e^3/m^2$. Therefore, theoretical predictions may be interesting and may give further insights into the strong correlations in the cuprates.

In summary, measurements of σ_{xy} in the infrared exhibit a nearly Drude behavior with a scattering rate linear in temperature, and only weakly frequency dependent, and a nearly temperature- and frequency-independent transverse spectral weight, which is only 0.09 of the band value. These results are in good agreement with calculations based on the fluctuation exchange model when current vertex corrections are included. Extending these IR Hall conductivity measurements over a wider frequency range in cuprates and other

strongly correlated electron systems may provide significant new insights into the physics of these materials in the vicinity of a Mott transition.

We wish to thank A.J. Millis, S. Das Sarma, and V.M. Yakovenko for their stimulating discussions. We also wish to thank D.B. Romero, who peeled and mounted the BSCCO sample. This work was supported by the NSF under Grant No. DMR-0030112 and by the DOE under Contract No. DE-AC02-98CH10886.

*Electronic address: schmadel@physics.umd.edu

¹Y. Sidis, S. Pailhes, B. Keimer, P. Bourges, C. Ulrich, and L. P. Regnault, *Phys. Status Solidi B* **241**, 1204 (2003).

²A. Damascelli, Z. Hussain, and Z. X. Shen, *Rev. Mod. Phys.* **75**, 473 (2003).

³A. J. Millis, A. Zimmers, R. P. S. M. Lobo, N. Bontemps, and C. C. Homes, *Phys. Rev. B* **72**, 224517 (2005).

⁴A. Zimmers, D. C. S. L. Shi, W. M. Fisher, R. L. Greene, H. D. Drew, G. A. M. Houseknecht, M.-H. Kim, M.-H. Yang, J. Černe, J. Lin *et al.*, cond-mat/0510085 (unpublished).

⁵T. Timusk and B. Statt, *Rep. Prog. Phys.* **62**, 61 (1999).

⁶H. Kontani and K. Yamada, *J. Phys. Soc. Jpn.* **74**, 155 (2005).

⁷H. Kontani, *J. Phys. Soc. Jpn.* **75**, 013703 (2006).

⁸J. Černe, M. Grayson, D. C. Schmadel, G. S. Jenkins, H. D. Drew, R. Hughes, A. Dabkowski, J. S. Preston, and P. J. Kung, *Phys. Rev. Lett.* **84**, 3418 (2000).

⁹J. Černe, D. C. Schmadel, L. B. Rigal, and H. D. Drew, *Rev. Sci. Instrum.* **74**, 4755 (2003).

¹⁰G. D. Gu, K. Takamuku, K. N. and S. Tanaka, *J. Cryst. Growth*, **130**, 325 (1993).

¹¹M. Grayson, L. B. Rigal, D. C. Schmadel, H. D. Drew, and P.-J. Kung, *Phys. Rev. Lett.* **89**, 037003 (2002).

¹²J. J. Tu, C. C. Homes, G. D. Gu, D. N. Basov, and M. Strongin, *Phys. Rev. B* **66**, 144514 (2002).

¹³H. D. Drew and P. Coleman, *Phys. Rev. Lett.* **78**, 1572 (1997).

¹⁴H. Kontani, cond-mat/0507664 (unpublished).

¹⁵D. van der Marel, H. J. A. Molegraaf, J. Zaanen, Z. Nussinov, F. Carbone, A. Damascelli, H. Eisaki, M. Greven, P. H. Kes, and M. Li, *Nature (London)* **425**, 271 (2003).

¹⁶M. A. Quijada, D. B. Tanner, R. J. Kelley, M. Onellion, H. Berger, and G. Margaritondo, *Phys. Rev. B* **60**, 14917 (1999).